Journal of Physics D: Applied Physics, 2016, 49 (24), pp 245003

DOI: 10.1088/0022-3727/49/24/245003

Interfacial tailoring exchange coupling of perpendicular magnetized Co/$L1_0$-$Mn_{1.5}Ga$ bilayers

J. X. Xiao[1], J. Lu[1], W. Q. Liu[2], Y. W. Zhang[1], H. L. Wang[1], L. J. Zhu[1], H. X. Deng[1,], D. H. Wei[1], Y. B. Xu[2], J. H. Zhao[1,†]*

[1]State Key Laboratory of Superlattices and Microstructures, Institute of Semiconductors, Chinese Academy of Sciences, P.O. Box 912, Beijing 100083, China

[2] Spintronics and Nanodevice Laboratory, Department of Electronics, University of York, York YO10 5DD, UK

Abstract: We have studied the magnetic properties of Co (2-12 MLs) /$L1_0$-$Mn_{1.5}Ga$ (15 nm) bilayers without and with annealing at 300 °C by a combination of superconducting quantum interference device (SQUID) magnetometry and x-ray magnetic circular dichroism (XMCD). We find that the Co layer can maintain perpendicularly magnetized when its thickness is less than 6 monolayers due to the coupling between Co and $L1_0$-$Mn_{1.5}Ga$ layers, which is double confirmed by both SQUID and XMCD measurements. Such an exchange coupling between $L1_0$-$Mn_{1.5}Ga$ and Co layers changes from ferromagnetic coupling to antiferromagnetic coupling after the annealing process. Furthermore, the magnetic coupling can also be tailored from ferromagnetic to antiferromagnetic by changing the $L1_0$-$Mn_{1.5}Ga$ surface from Mn-rich to Ga-rich. The first-principles calculations show that Mn-terminated $L1_0$-$Mn_{1.5}Ga$ bilayer is ferromagnetically coupled, while antiferromagnetically for Ga-terminated bilayer. The spin and orbital moments of Co in the Co/$L1_0$-$Mn_{1.5}Ga$ bilayers are calculated according to the sum rules and the ratio of the orbital to spin magnetic moments for Co is not enhanced like other perpendicularly magnetized Co-based multilayers such as Co/Pd and Co/Pt.

Keywords: Exchange interactions, Magnetic anisotropy, Spintronics, Molecular-beam epitaxy

PACS numbers: 71.70.Gm, 75.30.Gw, 85.75.-d, 81.15.Hi

Email: hxdeng@semi.ac.cn; jhzhao@red.semi.ac.cn

1. Introduction

Materials with large perpendicular magnetic anisotropy (PMA) have drawn great attention because of their potential applications in advanced spintronic devices such as spin-transfer-torque magnetic random access memory (STT-MRAM) and ultrahigh-density perpendicular magnetic recording [1,2]. To date, a large variety of PMA materials have been investigated, such as $L1_0$-ordered FePt, CoPt granular films [3-5], Co/(Pt,Pd,Ni) multilayers [6,7], ultra-thin CoFeB alloy and perpendicularly magnetized Co_2FeAl film [8]. Among the various kinds of materials with PMA, MnGa films with $L1_0$-structure have attracted much interest because of their large PMA (K_u~10^7erg/cm^3) [9-12], ultralow Gilbert damping constant of 0.008 [13] and theoretically predicted high spin polarization of more than 70% [9,14,15]. All these properties make $L1_0$-ordered MnGa a good candidate for low-critical-current STT-MRAM [16]. Recently, our group successfully synthesized rare-earth- and noble-metal-free $L1_0$-$Mn_{1.5}Ga$ films epitaxied on GaAs (001) substrates with large PMA, moderate magnetization, high coercivity and large magnetic energy product [17]. Moreover, the entire molecular-beam epitaxy (MBE) process is kept under 250 °C, which is advantageous for semiconductor device manufacturing process. However, MnGa-based magnetic tunnel junctions (MTJs) with a large tunnel magnetoresistance (TMR) have not been reported so far and the lattice mismatch between MnGa and MgO is a major problem [18,19]. Inserting a thin body-centered-cubic (bcc) structured layer of conventional 3*d* ferromagnetic metal or alloy, such as Fe, Co, CoFeB and CoFe, between the MnGa and the insulator layer, has proved to be a simple but effective means to improve the TMR [5,20,21]. Recently, Co insertion between MnGa and MgO was reported by Ma *et al* [22], in which the TMR ratio was enhanced from 5% (18%) to 40% (80%) at 300 K (5 K), and the Co insertion layer was shown to be antiferromagnetically (AFM) coupled with the MnGa layer, which is opposite to the case of Fe/MnGa reported by Kubota *et al* [23]. In this work, the perpendicularly magnetized Co/$L1_0$-$Mn_{1.5}Ga$ bilayers with different Co thickness have been studied by a combination of both superconducting quantum interference device (SQUID) magnetometer and x-ray magnetic circular dichroism (XMCD). The exchange coupling between $L1_0$-$Mn_{1.5}Ga$ and Co layers has changed from ferromagnetic (FM) coupling to AFM coupling after the annealing process. Furthermore, the magnetic coupling can also be tailored from FM to AFM by changing the $L1_0$-$Mn_{1.5}Ga$ surface from Mn-rich to Ga-rich, which is consistent with the first-principles calculations results. Moreover, by calculating the orbital and spin magnetic moments an indication of the absence of enhancement of the Gilbert damping constant is observed in the Co/$L1_0$-$Mn_{1.5}Ga$ bilayers.

2. Experiments

All the Co/$L1_0$-$Mn_{1.5}Ga$ bilayers with varying thicknesses of Co layer (t_{Co}) were grown by the molecular-beam epitaxy system (VG80) with two growth chambers, and the entire growth was carried out under ultrahigh vacuum without any air exposure. The structure of the multilayer was Al (2 nm)/Co (t_{Co} MLs)/$L1_0$-$Mn_{1.5}Ga$ (15 nm)/GaAs (200 nm), deposited on a semi-insulating GaAs (001) single-crystal substrate. Firstly, about 3~5 monolayers (MLs) amorphous $Mn_{1.5}Ga$ seed layer was deposited on a smooth 200-nm thick GaAs buffer layer at a low temperature (less than 30 °C) to suppress the inter-diffusion and reaction, after that the sample was annealed *in situ* at 250 °C for 5 mins to crystallize the seed layer, and then 15 nm $L1_0$-$Mn_{1.5}Ga$ was deposited onto the seed layer at a substrate temperature of 250 °C with streaky reflection high-energy electron diffraction (RHEED) patterns observed, which implied high crystalline quality and a smooth surface for the $L1_0$-$Mn_{1.5}Ga$ layer. Next, an ultrathin Co layer with different thickness (t_{Co} = 2, 4, 6, 9 and 12 MLs) was deposited at room temperature to minimize the inter-diffusing at the interface. Finally, a 2 nm Al layer was deposited at room temperature to prevent oxidation. During the growth of the Co layer, a structure transformation from bcc to hexagonal-closed-packed (hcp) was observed from the change of RHEED patterns when t_{Co} was beyond 9 MLs. A similar phenomenon was also reported in Co/GaAs (001) system by Wu *et al* [24].

Both the in-plane and out-of-plane magnetization of the Co/$L1_0$-$Mn_{1.5}Ga$ bilayers were measured in the magnetic field range of ±50 kOe using the SQUID. Since the hysteresis loops measured by SQUID represent the magnetization information of the entire Co/$L1_0$-$Mn_{1.5}Ga$ bilayer, the element-specific XMCD measurements were also performed at Diamond Light Source in the UK, by which the magnetic properties of Co layer and $L1_0$-$Mn_{1.5}Ga$ layer could be measured individually.

3. Results and discussion

3.1. Magnetization behaviors of Co/$L1_0$-$Mn_{1.5}Ga$ bilayers

The typical in-plane and out-of-plane hysteresis loops (*M-H* curves) of Al/Co/$L1_0$-$Mn_{1.5}Ga$/GaAs films with a 4 MLs Co layer are given in figure 1(*a*). A nearly square shaped loop is observed from the out-of-plane *M-H* curve, however the in-plane curve is almost hysteresis-free with close to zero remnant magnetization (M_r), which clearly evidences the PMA of this Co/$L1_0$-$Mn_{1.5}Ga$ bilayer. Figure 1(*b*) shows the out-of-plane *M-H* curves of Co/$L1_0$-$Mn_{1.5}Ga$

bilayers with different t_{Co}. It is obvious that the out-of-plane magnetization becomes more difficult to saturate as t_{Co} increases, and the saturation field exceeds 25 kOe for the sample with t_{Co} =12 MLs. Such a t_{Co} dependence are summarized in figure 1(*c*) and (*d*). With increasing t_{Co}, the saturation magnetization (M_s, black squares) linearly increases due to the contribution of Co layer. By fitting the M_s-t_{Co} dependence, the atomic moment of Co layer can be extracted as 1.21 μ_B/atom, which is consistent with the reported values in similar system [25]. In contrast to the increasing M_s, the ratio of M_r/M_s continually drops from 0.91 to 0.60 (blue dots). It indicates the gradual rotation of easy magnetization axis from out-of-plane to in-plane as t_{Co} increases. Figure 1(*d*) summarizes the M_r values for the Co/$L1_0$-$Mn_{1.5}Ga$ bilayers without annealing process. The M_r increases with increasing t_{Co} up to 6 MLs, which is probably due to the ferromagnetic coupling (FM) between the Co and $L1_0$-$Mn_{1.5}Ga$ layers. When t_{Co} > 6 MLs the magnetization of Co layer gradually rotates into the film plane and its contribution to the total out-of-plane magnetization getting smaller, which makes the M_r decreases, and we will demonstrate and explain them via XMCD measurements in depth.

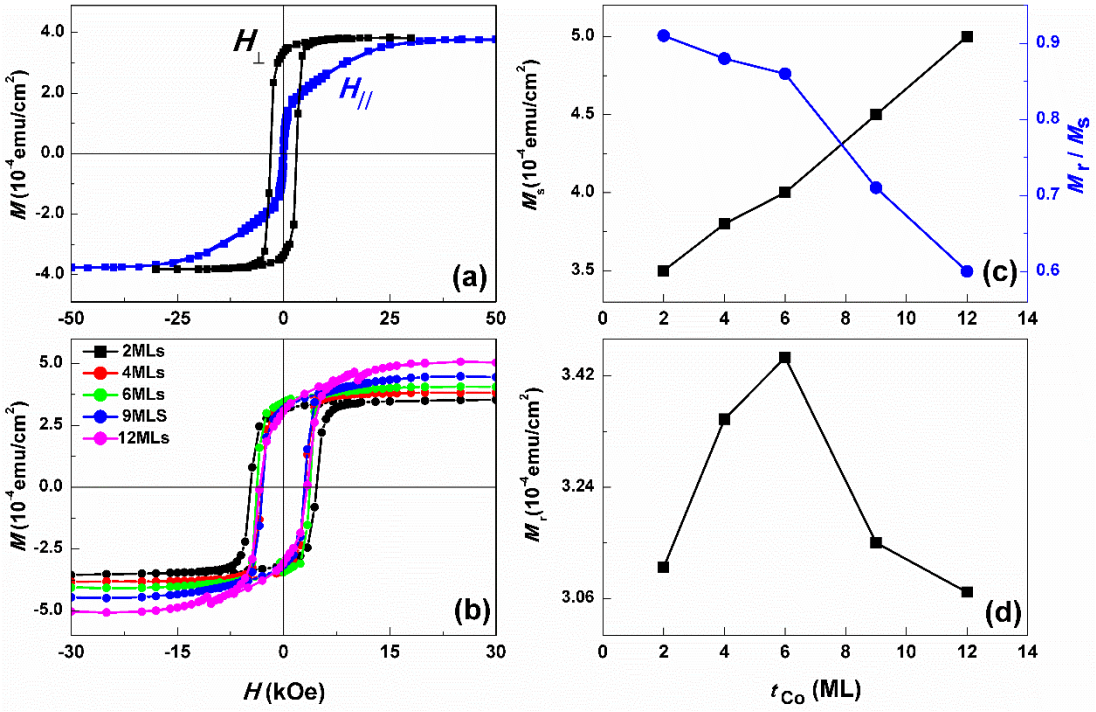

Figure 1. (a) In-plane and out-of-plane *M-H* loops for an Al/Co/$L1_0$-$Mn_{1.5}Ga$/GaAs film with t_{Co} = 4 MLs. (b) Out-of-plane *M-H* loops of Al/Co/$L1_0$-$Mn_{1.5}Ga$/GaAs films, with the Co thickness *t* = 2, 4, 6, 9 and 12 MLs. (c) Dependence of M_s and M_r/M_s on the Co thickness. (d) Dependence of M_r on the Co thickness.

The variation of PMA of the Co layer versus t_{Co} can also be seen from the in-plane and out-of-plane *M-H* curves for Co/$L1_0$-$Mn_{1.5}Ga$ bilayers with t_{Co} = 2, 6, 9 and 12 MLs, as shown in

figure 2. When t_{Co} is 2 MLs, there is almost no hysteresis for the in-plane *M-H* curve with almost zero M_r; while above 6 MLs, the hysteresis begins to be clear. It implies that the easy magnetization axis of the Co layer is perpendicular to the film plane for samples with Co layer less than 6 MLs, and then gradually rotates into the film plane as t_{Co} increases. This conclusion is also consistent with the XMCD measurements as shown below.

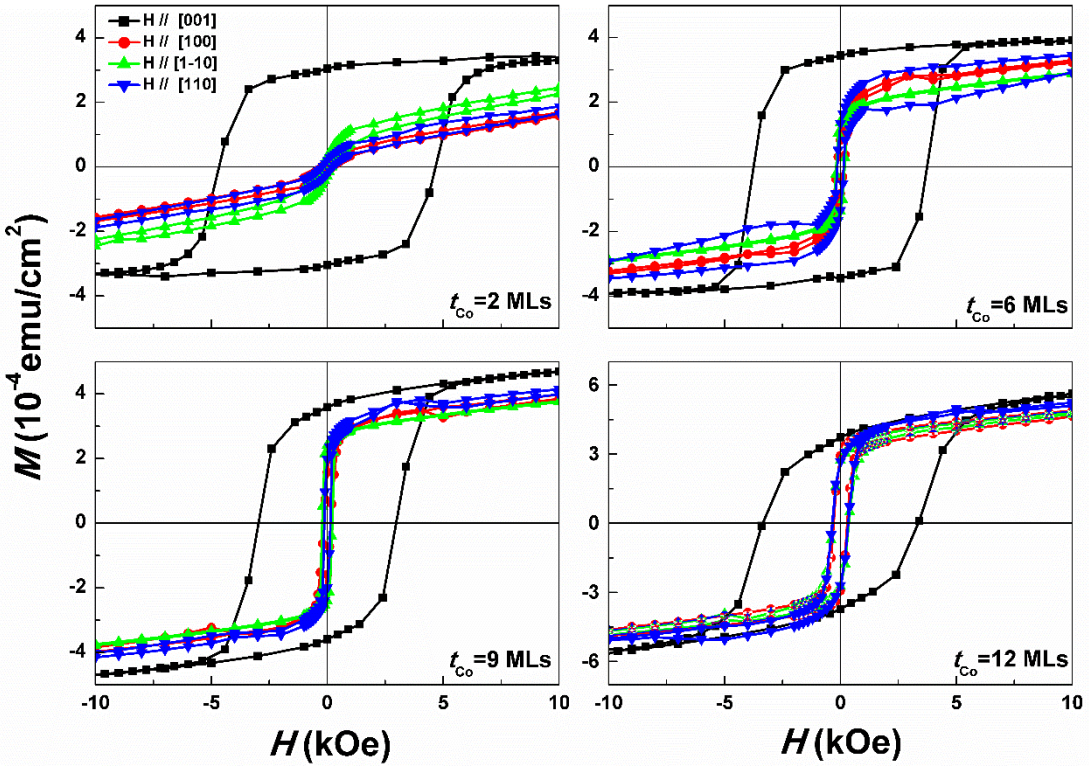

Figure 2. In-plane and out-of-plane *M-H* loops for Al/Co/$L1_0$-$Mn_{1.5}Ga$/GaAs films with the Co thickness t = 2, 6, 9 and 12 MLs.

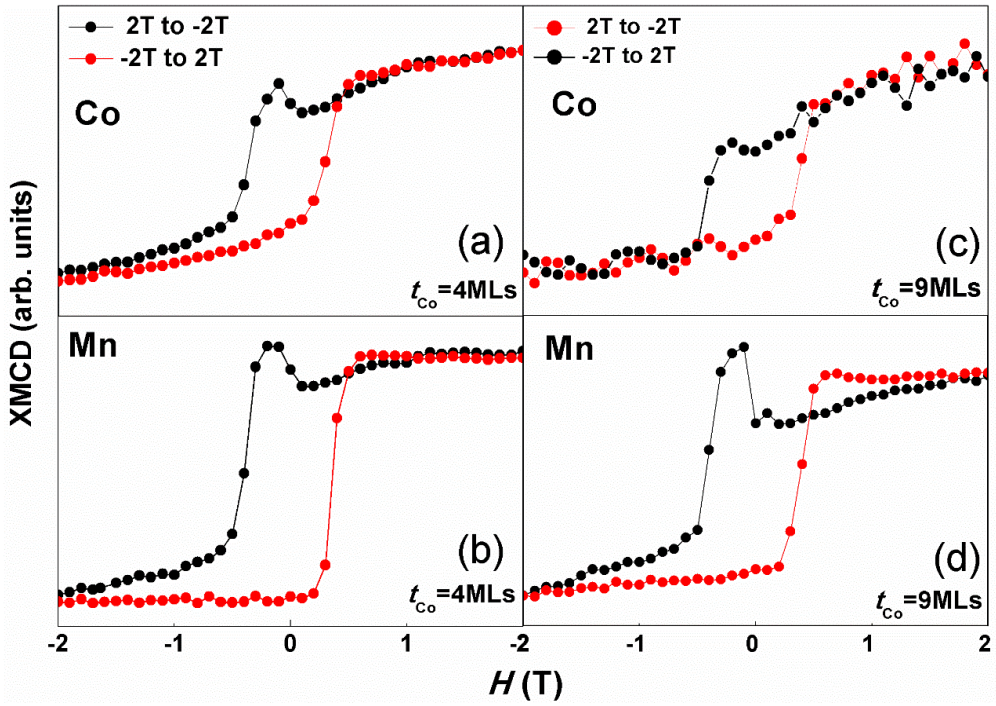

Figure 3. Element specific XMCD loops for (a) Co, (b) Mn, measured for unannealed sample Al/Co/$L1_0$-$Mn_{1.5}Ga$/GaAs with t_{Co} = 4 MLs, and (c) Co, (d) Mn, measured for unannealed sample Al/Co/$L1_0$-$Mn_{1.5}Ga$/GaAs with t_{Co} = 9 MLs, and all the loops were measured with the magnetic field perpendicular to the film plane.

3.2. Element-specific XMCD hysteresis loops of Co/$L1_0$-$Mn_{1.5}Ga$ bilayers

Though the FM coupling between Co and $L1_0$-$Mn_{1.5}Ga$ layers has been implied by SQUID measurements, here we show direct evidence from XMCD measurements. The measurements were performed by detecting the external field-dependent transmitted intensity of the circularly polarized soft X-rays with the energy set to the experimental L_3 resonant edges of Co (780.4 eV) and Mn (640.0 eV). It has an advantage of element-specific, which can individually measure the magnetization of Co and Mn separately. The element-specific XMCD hysteresis loops of the Co/$L1_0$-$Mn_{1.5}Ga$ bilayers with different Co thickness (4 MLs and 9 MLs) are shown in figure 3. All loops were measured in the perpendicular configuration in a magnetic field range of ±2 T, while the top (bottom) panels are for Co (Mn), and the left (right) panels for a Co thickness of 4 MLs (9 MLs) respectively. As a comparison at 4 MLs and 9 MLs, both Co and Mn are perpendicularly magnetized with same polarity and almost the same coercivity, which is consistent with that measurement by SQUID. All these results have clearly shown that the Co and $L1_0$-$Mn_{1.5}Ga$ are ferromagnetically coupled. Moreover, for the Co loops, it is not so square when t_{Co} = 9 MLs (figure 3(*c*)) compared with 4 MLs (figure 3(*a*)), which means the magnetic

moment of Co gradually deviates from perpendicular direction as the Co thickness increases from 4 MLs to 9 MLs. What's more, these results unambiguously corroborate the variation of M_r versus t_{Co} measured by SQUID, as summarized in figure 1(*d*). Our observation is different from the AFM coupling results between Co and $L1_0$-$Mn_{1.5}Ga$ layers that reported by Ma *et al* [22]. The possible reason for this difference is the post-growth annealing effect. The Co layer in our samples was deposited at room-temperature without post-growth annealing process which can suppress the undesired inter-diffusion to a large extent. This explanation is also supported by the result reported lately by Ranjbar *et al* [26], though their main results are obtained by magneto optical Kerr effect (MOKE).

In order to verify the effect of annealing process, the *ex situ* annealing treatment was performed for the Co/$L1_0$-$Mn_{1.5}Ga$ bilayers at 300 °C in pure N_2 atmosphere for 20 minutes. Figure. 4 is the XMCD loops of Co and Mn for the annealed samples, from the figure, the Co of annealed Co/$L1_0$-$Mn_{1.5}Ga$ bilayers show inverted loops compared with the unannealed bilayers, while the loops of Mn have the same trend. The change of the Co loops definitely proves that the coupling between Co and $L1_0$-$Mn_{1.5}Ga$ has transformed from FM coupling to AFM coupling after the annealing process.

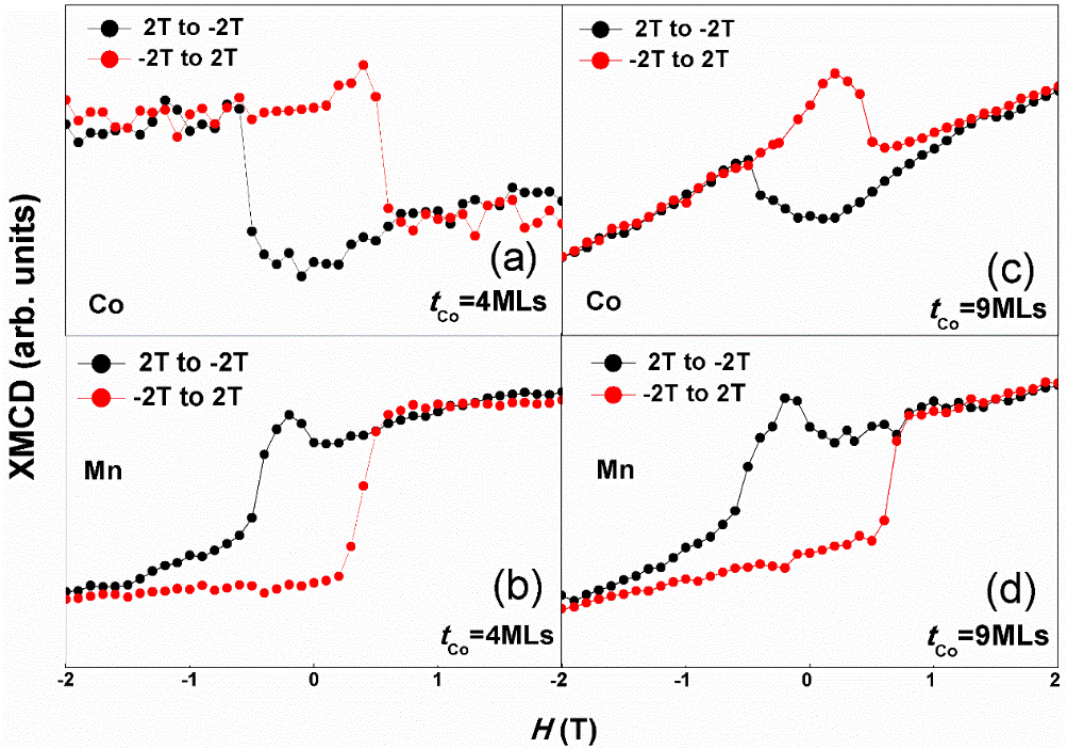

Figure 4. Element specific XMCD loops for (a) Co, (b) Mn, measured for annealed sample Al/Co/$L1_0$-$Mn_{1.5}Ga$/GaAs with t_{Co} = 4 MLs, and (c) Co, (d) Mn, measured for annealed sample

Al/Co/$L1_0$-$Mn_{1.5}Ga$/GaAs with t_{Co} = 9 MLs, and all the loops were measured with the magnetic field perpendicular to the film plane.

3.3. The first-principles calculations of coupling between Co and $L1_0$-$Mn_{1.5}Ga$

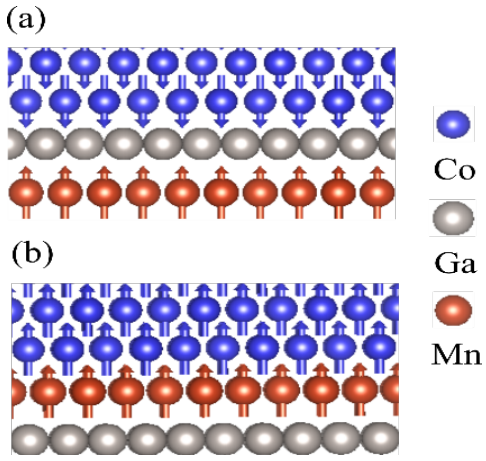

Figure. 5 Schematic interfacial structures for (a) Ga-Co interface for the AFM interlayer coupling, and (b) Mn-Co interface for the FM interlayer coupling between Co and $L1_0$-$Mn_{1.5}Ga$ layers.

To analyze the physical origin of the magnetic phase transition after the annealing process, we calculated the interfacial binding energy (IBE): $E_{IBE}^{S} = E_{int}^{S} - (E_{GaMn} + E_{Co})$ of Co/$L1_0$-$Mn_{1.5}Ga$ interface in the interlayer coupling state *S* (FM or AFM coupling) (as shown in figure 5), where E_{GaMn} and E_{Co} are the total energies of the $L1_0$-$Mn_{1.5}Ga$ and Co slabs with free surfaces, respectively, E_{int}^{S} is the total energy of the Co/$L1_0$-$Mn_{1.5}Ga$ supercell slab embedded in vacuum with interlayer coupling state *S*. The total energy calculations are carried out in the framework of the density functional theory (DFT) [27,28], as implemented in the *Vienna ab initio simulation package* (VASP) [29-31]. Due to the fact that the Co layer experimentally has a bcc structure grown on $L1_0$-$Mn_{1.5}Ga$, we construct an interfacial slab model that the bcc Co lattice is strained to fit on the (001) surface of the underlying $L1_0$-$Mn_{1.5}Ga$ lattice by rotating 45°, namely, the lattice between Co and MnGa has the orientation relationship of Co (001)//MnGa (001) and Co [110]//MnGa [100] in the directions perpendicular and parallel to the interface, respectively. In this case, the lattice mismatch between $L1_0$-$Mn_{1.5}Ga$ and Co layers is very small and only 1.04 %. The thickness perpendicular to interface is up to 5 MLs both for $L1_0$-$Mn_{1.5}Ga$ and Co layers in the simulations. In the calculations, all the atoms are allowed to relax until the quantum mechanical forces acting on them become less than 0.02 eV/Å. From the

calculated results, we find, for the Ga-Co interfaces (figure. 5(*a*)), the energy difference $\Delta E_{IBE}^{FM-AFM} = E_{IBE}^{FM} - E_{IBE}^{AFM}$ of IBE between FM and AFM interlayer coupling is about 3 meV per 4 atoms, and the AFM coupling interface is more stable. However, for the Mn-Co interface (figure. 5(*b*)), the calculated difference ΔE_{IBE}^{FM-AFM} is -46 meV per 4 atoms, and the FM coupling interface is more stable. Moreover, since the Ga-Co bond is more stable than the Mn-Co bond, the Ga-Co interface is more stable than the Mn-Co interface at low temperature. Therefore, after the annealing, the interfacial structure could opt for the Ga-Co interface. This is the reason why the magnetic phase changes from FM to AFM coupling after the annealing process.

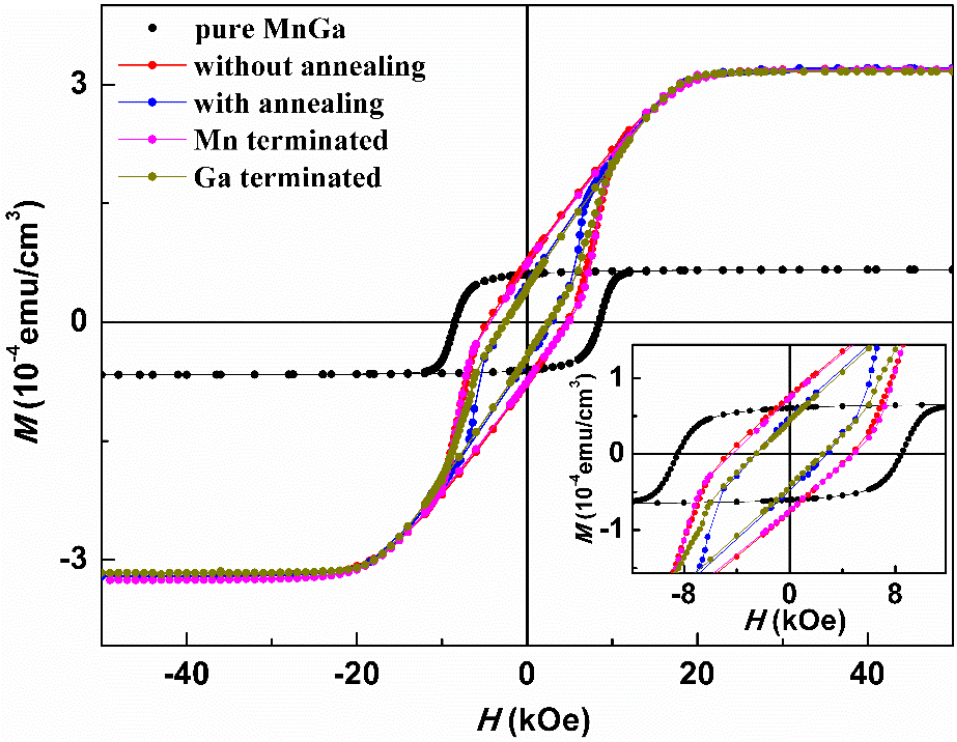

Figure 6. Out-of-plane *M-H* curves for sample 1, sample 2, sample3, sample 4 and the reference sample, and detailed information is marked in the figure.

To further verify the calculated results, 4 samples with a main stacking structure of Al (2 nm)/Co (20 nm)/$L1_0$-$Mn_{1.5}Ga$ (20 nm)/GaAs (200 nm) were fabricated, $L1_0$-$Mn_{1.5}Ga$ layers of sample 1 (2) has Mn (Ga) rich surface by depositing extra 1-2 MLs Mn or Ga prior to the deposition of Co layer without any annealing process. Sample 3 and sample 4 have the same stacking structure but without interfacial tailoring, and sample 4 is annealed *in situ* after the Co

layer deposition. In additional, a bare 20 nm-thick $L1_0$-$Mn_{1.5}Ga$ film without Co layer was fabricated as reference sample. Figure. 6 is the out-of-plane *M-H* curves that corresponding to these samples. From the figure, the M_r value for Co/$L1_0$-$Mn_{1.5}Ga$ bilayers without annealing process and bilayers with a Mn-rich interface increases compared with the pure $L1_0$-$Mn_{1.5}Ga$ films due to the FM coupling, while the M_r value for annealed Co/$L1_0$-$Mn_{1.5}Ga$ bilayers and bilayers with a Ga-rich interface decreases because of the AFM coupling. We marked the magnetic field with H_{ex} corresponding to the state that $L1_0$-$Mn_{1.5}Ga$ films is perpendicularly magnetized while Co layer is completely in plane magnetized, and AFM coupling exists when H_{ex} is positive while FM coupling for negative H_{ex}. The H_{ex} values for different samples are given in table 1, and the results indicate that Mn-terminated Co/$L1_0$-$Mn_{1.5}Ga$ bilayer is more likely to form FM coupling, but AFM coupling for Ga-terminated bilayer, which is in consistent with the theoretical predictions. Meanwhile, the exchange coupling between Co and $L1_0$-$Mn_{1.5}Ga$ has changed from FM coupling to AFM coupling after the annealing process, which is also consistent with the XMCD results discussed in session 3.2, and the interfacial structure rearrangement is the possible reason for the change.

sample	Sample 1	Sample 2	Sample 3	Sample 4
H_{ex}	-0.82 kOe	1.04 kOe	-1.05 kOe	0.80 kOe

Table 1 H_{ex} for different samples obtained from the out-of-plane *M-H* curves

3.4. XMCD spectra of Co/$L1_0$-$Mn_{1.5}Ga$ bilayers

The Gilbert damping constant *G* that is critically sensitive to the spin-orbit coupling is an important factor for the application of STT-MRAM. Couplings between neighboring layers can modify both spin- and orbital- moments, which would change *G* for the multilayers. According to the following equations mentioned by Pelzl *et al* [32],

$$G = \left(\frac{\gamma}{2}\right)^2 Z_F \lambda_{SO}^2 (g-2)^2 \tau \qquad (1)$$

$$g - 2 = 2\frac{\mu_L}{\mu_s} \qquad (2)$$

Where μ_L, μ_S are the orbital- and spin- moments, γ the gyro-magnetic ratio, λ_{SO} the spin-orbital-coupling constant, Z_F the density of states at the Fermi level, τ the electron scattering time and g the Lande's factor, respectively, the damping constant G varies with the square of the ratio of orbital-to-spin magnetic moment. Hence the values ofμ_L andμ_S can provide information about the damping constant of the material or multilayer. The sum rules was first introduced theoretically in early 1990s, to provide a way to deduce element-specific orbital and spin magnetic moments from the integrals of experimentally derived x-ray absorption spectra (XAS) and its associated XMCD spectra [33-35].

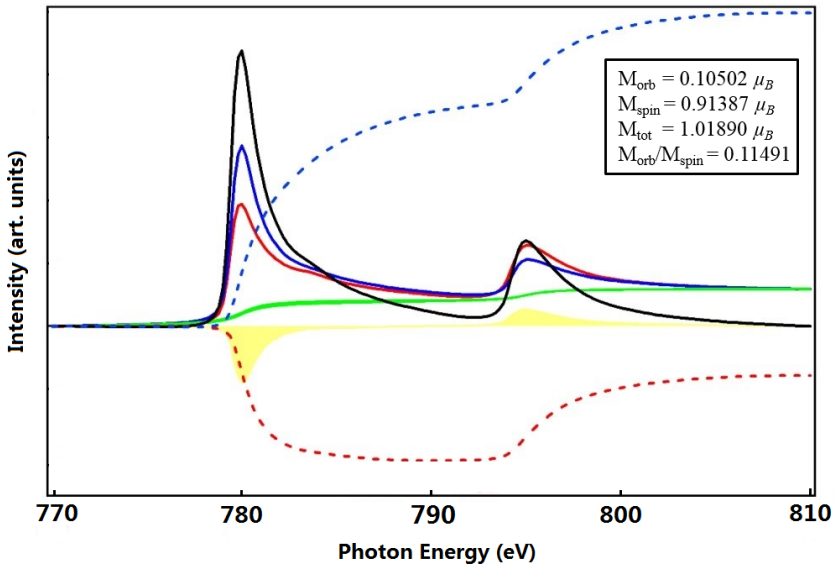

Figure 7. The deduced spin and orbital moments for Co of unannealed Co/$L1_0$-$Mn_{1.5}Ga$ bilayer with 4 MLs Co. The blue and red solid lines are absorption spectra for right and left circularly polarized x-rays, respectively. The yellow solid line is the XMCD spectra obtained from the difference between the absorption spectra and the red dashed line is the integration of the XMCD spectra. The black solid line is the sum of the two absorption spectra, while the blue dashed line represents the integration of the summed spectra.

In this work, we performed XAS measurements for annealed and unannealed Co/$L1_0$-$Mn_{1.5}Ga$ bilayers with t_{Co} = 4 MLs and 9 MLs respectively, and both the spin and orbital moments of Co were calculated according to the sum rules. Figure 7 illustrates the spin and orbital moments results of Co for unannealing Co/$L1_0$-$Mn_{1.5}Ga$ bilayer with t_{Co} = 4 MLs calculated from the XAS data, and the values for other samples are obtained in the same way. All the values obtained in our experiments are summarized in table 3 together with the values reported before. From the table, the orbital moments of Co in the Co/$L1_0$-$Mn_{1.5}Ga$ bilayers are

not enhanced like that of Co in Co/Pd and Co/Pt [36,37]. Especially, the ratio of μ_L/μ_S is almost the same as that of bulk Co. According to Pelzl's theory, the smaller ratio of μ_L/μ_S implies smaller G, so low G in the Co/$L1_0$-$Mn_{1.5}Ga$ bilayer should be expected, which makes Co/$L1_0$-$Mn_{1.5}Ga$ bilayers a good candidate material for STT-MRAM applications.

	Co			
	μ_L	μ_S	μ_L/μ_S	References
Co	0.13	-----	-----	37
Co/Ni	0.13	-----	-----	
Co/Pd	0.28	-----	-----	
Co/Pt	0.20	-----	-----	
Co	0.13	-----	-----	36
Co/Pt	0.25	-----	-----	
Co	0.154	1.62	0.095	35
Co/MnGa	0.10502	0.91387	0.11491	4MLs-No annealing
	0.10606	0.90861	0.11673	4MLs-Annealing
	0.12858	1.2332	0.10426	9MLs-No annealing
	0.09043	0.8697	0.10398	9MLs-Annealing

Table 2 Orbital and spin moments for Co in units of μ_B/atom

4. Conclusions

In summary, we have fabricated Co/$L1_0$-$Mn_{1.5}Ga$ bilayers with different Co thickness by MBE and investigated their magnetic properties via SQUID and XMCD measurements. The perpendicular magnetization of the ultrathin Co layers was verified in the bilayers when the thickness of the Co layer was less than 6 MLs. Moreover, the coupling between the Co and $L1_0$-$Mn_{1.5}Ga$ was confirmed unambiguously to change form FM coupling to AFM coupling after annealing process or intended interfacial tailoring. The spin and orbital moments of Co in the Co/$L1_0$-$Mn_{1.5}Ga$ bilayers were also calculated according to the sum rules, and no enhancement was found for either μ_L or μ_L/μ_S of Co in the Co/$L1_0$-$Mn_{1.5}Ga$ bilayer in contrast to the Co/Pt or Co/Pd systems. This probably implies that there is no enhancement of the damping constant in the Co/$L1_0$-$Mn_{1.5}Ga$ system, which is important for achieving high-speed and low critical current density spin torque transfer magnetization switching.

Acknowledgments

Diamond Light Source is acknowledged for beamtime on I10, and we also acknowledge Peng Xiong at Florida State University for useful discussion. The work was supported by the National High-tech R&D Program of China [MOST, Grant Nos. 2014AA032904], National Program on Key Basic Research Project [MOST, Grant Nos. 2015CB921500] and the National Natural Science Foundation [NSFC, Grant Nos. 61334006, 11304307, 11474273]. Diamond Light Source is acknowledged to I10.

References

[1] Yoda H *et al*. 2010 *Curr*. *Appl*. *Phys*. **10**, E87

[2] Weller D, Moser A, Folks L, Best M E, Lee W, Toney M F, Schwickert M, Thiele J-U, and Doerner M F 2000 IEEE *Trans*. *Magn*. **36** 10

[3] Seki T, Mitani S, Yakushiji K, and Takanashi K 2006 *Appl*. *Phys*. *Lett*. **88**, 172504

[4] Kim G, Sakuraba Y, Oogane M, Ando Y, and Miyazaki T 2008 *Appl*. *Phys*. *Lett*. **92**, 172502

[5] Yoshikawa M, Kitagawa E, Nagase T, Daibou T, Nagamine M, Nishiyama K, Kishi T, and Yoda H 2008 IEEE *Trans*. *Magn*. **44**, 2573

[6] Yakushiji K, Saruya T, Kubota H, Fukushima A, Nagahama T, Yuasa S, and Ando K 2010 *Appl*. *Phys*. *Lett*. **97**, 232508

[7] Mizunuma K, Yamanouchi M, Ikeda S, Sato H, Yamamoto H, Gan H D, Miura K, Hayakawa J, Matsukura F, and Ohno H 2011 *Appl*. *Phys*. *Express* **4**, 3002

[8] Wen Z C, Sukegawa H, Mitani S, and Inomata K 2011 *Appl*. *Phys*. *Lett*. **98**, 242507

[9] Balke B, Fecher G H, Winterlik J, and Felser C, 2007 *Appl*. *Phys*. *Lett*. **90**, 152504

[10] Kurt H, Rode K, Venkatesan M, Stamenov P, and Coey J M D 2011 *Phys*. Status Solidi B

248, 2338

[11] Mizukami S, Kubota T, Wu F, Zhang X, Miyazaki T, Naganuma H, Oogane M, Sakuma A, and Ando Y 2012 *Phys. Rev. B* **85**, 014416

[12] Wu F, Mizukami S, Watanabe D, Naganuma H, Oogane M, Ando Y, and Miyazaki T 2009 *Appl. Phys. Lett.* **94**, 122503

[13] Mizukami S, Wu F, Sakuma A, Walowski J, Watanabe D, Kubota T, Zhang X, Naganuma H, Oogane M, and Ando Y 2011 *Phys. Rev. Lett.* **106**, 117201

[14] Winterlik J, Balke B, Fecher G H, Felser C, Alves M C, Bernardi F, and Morais J 2008 *Phys. Rev. B* **77**, 054406

[15] Bai Z Q , Cai Y Q, Shen L, Yang M, Ko V, Han G C, and Feng Y P 2012 *Appl. Phys. Lett.* **100**, 022408

[16] Nakayama M, Kai T, Shimomura N, Amano M, Kitagawa E, Nagase T, Yoshikawa M, Kishi T, Ikegawa S, and Yoda H 2008 *J. Appl. Phys.* **103**, 07A710

[17] Zhu L J, Nie S H, Meng K K, Pan D, Zhao J H, and Zheng H Z 2012 *Adv. Mater.* **24**, 4547

[18] Kubota T, Mizukami S, Watanabe D, Wu F, Zhang X M, Naganuma H, Oogane M, Ando Y, and Miyazaki T 2011 *J. Appl. Phys.* **110**, 013915

[19] Kubota T, Araidai M, Mizukami S, Zhang X M, Ma Q L, Naganuma H, Oogane M, Ando Y, Tsukada M, and Miyazaki T 2011 *Appl. Phys. Lett.* **99**, 192509

[20] Mizunuma K, Ikeda S, Park J H, Yamamoto H, Gan H, Miura K, Hasegawa H, Hayakawa J, Matsukura F, and Ohno H 2009 *Appl. Phys. Lett.* **95**, 232516

[21] Nakayama M, Kai T, Shimomura N, Amano M, Kitagawa E, Nagase T, Yoshikawa M, Kishi T, Ikegawa S, and Yoda H 2008 *J. Appl. Phys.* **103**, 07A710

[22] Ma Q L, Kubota T, Mizukami S, Zhang X M, Naganuma H, Oogane M, Ando Y, and

Miyazaki T 2012 *Appl. Phys. Lett.* **101**, 032402

[23] Kubota T, Ma Q L, Mizukami S, Zhang X M, Naganuma H, Oogane M, Ando Y, and Miyazaki T 2012 *Appl. Phys. Express* **5**, 043003

[24] Wu Y Z, Ding H F, Jing C, Wu D, Liu G L, Gordon V, Dong G S, Jin X F, Zhu S, and Sun K 1998 *Phys. Rev. B* **57**, 11935

[25] Blundell S J, Gester M, Bland J A C, Daboo C, Gu E, Baird M J and Ives A J R 1993 *J. Appl. Phys.* **73**, 5948

[26] Ranjbar R, Mizukami S, Ando Y, Kubota T, Ma Q L, Zhang X M, and Miyazaki T 2013 *J. Magn. Magn. Mater.* **346**, 53

[27] Kohn W and Sham L J 1965 *Phys. Rev.* **140**, A1133

[28] Hohenberg P and Kohn W 1964 *Phys. Rev.* **136**, B864

[29] Kresse G and Hafner J 1993 *Phys. Rev. B* **47**, 558

[30] Kresse G and Hafner J 1993 *Phys. Rev. B* **48**, 13115

[31] Kresse G and Furthmuller J 1996 *Comput. Mater. Sci.* 6, 15

[32] Pelzl J, Meckenstock J, Spoddig D, Schreiber F, Pflaum J and Frait Z 2003 *J. Phys. D: Appl. Phys* **15,** S451

[33] Thole B T, Carra P, Sette F, and van der Laan G 1992 *Phys. Rev. Lett.* **68**, 1943

[34] Carra P, Thole B T, Altarelli M, and Wang X D 1993 *Phys. Rev. Lett.* **70**, 694

[35] Chen C T, Idzerda Y U, Lin H J, Smith N V, Meigs G, Chaban E, Ho G H, Pellegrin E, and Sette F 1995 *Phys. Rev. Lett.* **75**, 152

[36] Wu Y, Stöhr J, Hermsmeier B D, Samant M G, and Weller D 1992 *Phys. Rev. Lett.* **69**, 2307

[37] Weller D, Wu Y, Stöhr J, Samant M G, Hermsmeier B D, and Chappert C 1994 *Phys. Rev. B* **49**, 12888